50th AIAA Aerospace Sciences Meeting including the New Horizons Forum and Aerospace Exposition
09 - 12 January 2012, Nashville, Tennessee

AIAA 2012-0609

Effects of mesh regularity on accuracy of finite-volume schemes

Boris Diskin* James L. Thomas†

The effects of mesh regularity on the accuracy of unstructured node-centered finite-volume discretizations are considered. The focus of this paper is on an edge-based approach that uses unweighted least-squares gradient reconstruction with a quadratic fit. Gradient errors and discretization errors for inviscid and viscous fluxes are separately studied according to a previously introduced methodology. The methodology considers three classes of grids: isotropic grids in a rectangular geometry, anisotropic grids typical of adapted grids, and anisotropic grids over a curved surface typical of advancing-layer viscous grids. The meshes within these classes range from regular to extremely irregular including meshes with random perturbation of nodes. The inviscid scheme is nominally third-order accurate on general triangular meshes. The viscous scheme is a nominally second-order accurate discretization that uses an average-least-squares method. The results have been contrasted with previously studied schemes involving other gradient reconstruction methods such as the Green-Gauss method and the unweighted least-squares method with a linear fit. Recommendations are made concerning the inviscid and viscous discretization schemes that are expected to be least sensitive to mesh regularity in applications to turbulent flows for complex geometries.

I. Introduction

Traditional mesh-quality metrics tend to assess meshes without taking into account the type of equations being solved, solutions, or the desired computational output. The most widely-used mesh quality metrics are geometric in nature, considering shape, size, angles, aspect ratio, skewness, Jacobian, etc., of the mesh elements. Additional considerations include variations between mesh elements, such as cell-to-cell and face-to-face ratios and line smoothness, etc. There is a widespread perception that the most accurate and efficient solutions are obtained on "pretty" meshes similar to either structured Cartesian meshes or to meshes composed from identical perfect elements (perfect triangles, tetrahedrals, etc.) This perception contradicts modern Computational Fluid Dynamics (CFD) practice, in which accurate solutions are computed on practical meshes that would be characterized as unacceptable by many geometric mesh quality metrics. Moreover, the most powerful state-of-art method for improving solution accuracy, output-based mesh adaptation,[1] tends to produce "ugly" meshes but provides vast improvements of the accuracy-per-degree-of-freedom ratio.[2] It is widely recognized today that mesh quality indicators should involve information about the solution[3–5] and, more generally, the discretization method in use and the desired computational output.

Historically, mesh quality analyses were first performed for finite-difference and finite-element methods. It is not straightforward to translate those approaches to finite-volume discretizations (FVD) that represent the state of art in CFD computations. While there is no doubt that certain mesh characteristics critically affect accuracy of CFD solutions and gradients, the precise nature of this influence (what affects what) is far from clear.

For finite-difference approaches, most of the mesh quality methods try to establish connections between mesh and truncation error.[6,7] The truncation error analysis is often applied to FVD schemes as well.[8] However, it has been long known, that truncation errors of FVD schemes on unstructured grids are not reliable estimators of discretization

*National Institute of Aerospace (NIA), 100 Exploration Way, Hampton, VA 23681, USA, Associate Fellow AIAA bdiskin@nianet.org. Also Department of Mechanical and Aerospace Engineering, University of Virginia, Charlottesville, VA 22904, USA. Supported by NASA Fundamental Aeronautics Program, Supersonics Project, NRA Contract NNL07AA23C (PI: Prof. N. K. Yamaleev).

†Computational AeroSciences Branch, NASA Langley Research Center, Mail Stop 128, Fellow AIAA, James.L.Thomas@nasa.gov.

errors. The *supra-convergence* of discretization errors observed and studied for at least 50 years (e.g., see the list of references in Ref. 8) indicates that design-order accurate FVD solutions can be computed on unstructured grids even when truncation errors exhibit a lower-order convergence or, in some cases, do not converge at all.[9–11]

The theory and applications of mesh quality assessments are well developed and widely used within the finite-element community. While groundbreaking work focused on pure geometrical mesh-quality metrics, such as large angles,[12,13] later developments take the solution into account.[14] The standard finite-element estimates use Sobolev norms that simultaneously estimate errors in the solution and its derivatives. These estimates might be too conservative because recent finite-volume computations indicate that accurate solutions can be obtained in spite of poor accuracy of gradients.[15–17]

Previously, the authors evaluated the effects of mesh regularity on accuracy of unstructured FVD schemes for various common node-centered and cell-centered schemes.[15,16,18–20] The considered second-order node-centered schemes employ three gradient reconstruction methods: unweighted and weighted least-squares (ULSQ and WLSQ, respectively) methods with a linear fit and a Green-Gauss (GG) method. The following observations concerning relations between accuracy and grid regularity have been made: (1) Convergence and magnitudes of truncation errors are strongly affected by grid regularity and often mislead in predicting convergence and magnitudes of discretization errors. (2) Some common inviscid FVD schemes, e.g., with WLSQ gradients, produce larger discretization errors (possibly diverging in grid refinement) on almost perfectly regular grids than on very irregular grids with the same degrees of freedom (DOF). This striking observation shows the futility of assessing mesh quality independently of the discretization scheme and motivates employment of more stable ULSQ methods. (3) Convergence and magnitude of discretization errors on isotropic grids are often independent of grid regularity. (4) Gradient accuracy may degrade on irregular high-aspect-ratio grids; effects of this degradation are much stronger on viscous solutions than on inviscid solutions. (5) Grid regularity may strongly affect convergence of iterative solvers, e.g., defect-correction iterations. (6) Stochastic tests may be required to account for variations introduced by outlier geometries on irregular grids.

The focus of this paper is on an edge-based node-centered approach. An FVD scheme is considered as edge-based if a loop over edges is sufficient to compute residuals of all equations.[21] Edge-based schemes offer advantages of efficiency (much more efficient than schemes that need to loop over elements in order to compute residuals and linearizations), generality (applicable to agglomeration grids with no explicit elements), and easier grid adaptation. Widely used node-centered FVD schemes[22] are edge-based for inviscid residuals on all grids and for viscous residuals on simplicial grids; viscous residuals on non-simplicial elements require an element loop. An attractive feature of an edge-based scheme for integrating fluxes over a median-dual control volume is that the integration is up to third-order accurate on general simplicial grids; the integration accuracy may degenerate to first order on general grids including non-simplicial elements.

There is computational evidence that second-order FVD schemes used for practical computations of turbulent flows demonstrate a better accuracy on mixed-element viscous grids with prismatic elements in boundary layers than on fully tetrahedral grids. This evidence is the main motivation for using mixed unstructured grids in spite of efficiency degradation caused by losing the edge-based character of the schemes. Recent publications[23,24] introduced an efficient edge-based FVD scheme using WLSQ gradient reconstruction with a quadratic fit and showed third-order accuracy for inviscid fluxes on general triangular grids. With this scheme, a comparable or even superior turbulent flow accuracy may be possible on fully tetrahedral grids.

This paper considers effects of mesh regularity on the accuracy of edge-based FVD schemes using ULSQ gradients computed with a quadratic fit. The inviscid scheme is nominally third-order accurate on general triangular meshes. The viscous scheme is a nominally second-order accurate discretization that uses an average-least-squares method. The schemes have been contrasted with previously studied schemes involving other gradient reconstruction methods such as the Green-Gauss method and the ULSQ method with a linear fit.

Gradient errors and discretization errors are separately studied according to a previously introduced comprehensive methodology.[15,16] A linear convection equation,

$$(\mathbf{a} \cdot \nabla) U = f, \tag{1}$$

with a velocity vector, $\mathbf{a}$, serves as a model for inviscid fluxes. Poisson's equation

$$\Delta U = f, \tag{2}$$

subject to Dirichlet boundary conditions serves as a model for viscous fluxes. The method of manufactured solutions is used. Solutions are chosen to be smooth on all grids considered, i.e., no accuracy degradation occurs because of a lack of solution smoothness.

The paper is organized as following. First, grids, FVD schemes, and accuracy measures are briefly described. Then, numerical studies of the FVD accuracy measures are reported for grids of three classes representing isotropic, adapted, and turbulent-flow grids. Finally, conclusions and recommendations are offered concerning the FVD schemes that are expected to be least sensitive to mesh regularity in applications to turbulent flows in complex geometries. Appendix A illustrates high sensitivity of truncation errors to grid regularity. Appendix B presents a study of gradient accuracy as a function of grid deformation typical for curved anisotropic grids used in turbulent-flow computations.

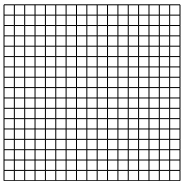

(a) **Type (I): regular quadrilateral grid.**

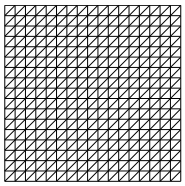

(b) **Type (II): regular triangular grid.**

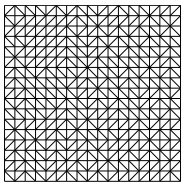

(c) **Type (III): random triangular grid.**

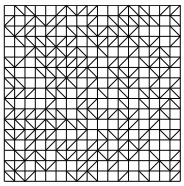

(d) **Type (IV): random mixed grid.**

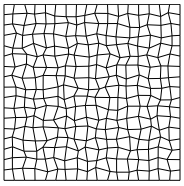

(e) **Type (I_p): perturbed quadrilateral grid.**

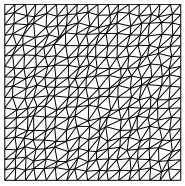

(f) **Type (II_p): perturbed triangular grid.**

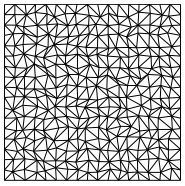

(g) **Type (III_p): perturbed random triangular grid.**

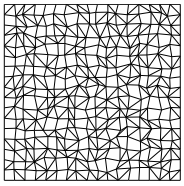

(h) **Type (IV_p): perturbed random mixed grid.**

Figure 1. Class A: regular and irregular grids.

II. Grid Classes and Types

Computational studies are conducted on two-dimensional grids ranging from structured (regular) grids to irregular grids composed of arbitrary mixtures of triangles and quadrilaterals. Highly irregular grids are deliberately constructed through random perturbations of structured grids. Three classes of grids are considered. Class A involves isotropic grids in a rectangular geometry. Class B involves highly anisotropic grids in a rectangular geometry, typical of those encountered in grid adaptation. Class C involves advancing-layer grids varying strongly anisotropically over a curved geometry, typical of those encountered in high-Reynolds number turbulent flow simulations.

Four basic grid types are considered: (I) *regular quadrilateral* (i.e., mapped Cartesian) grids; (II) *regular triangular grids* derived from the regular quadrilateral grids by the same diagonal splitting of each quadrilateral; (III)

random triangular grids, in which regular quadrilaterals are split by randomly chosen diagonals, each diagonal orientation occurring with a probability of half; and (IV) *random mixed-element grids*, in which regular quadrilaterals are randomly split or not split by diagonals; the splitting probability is half; in case of splitting, each diagonal orientation is chosen with probability of half. Nodes of any basic-type grid can be perturbed from their initial positions by random shifts, thus leading to four additional *perturbed* grid types which are designated by the subscript p as (I_p)-(IV_p). The random node perturbation in each dimension is typically defined as $\frac{1}{4}\rho h$, where $\rho \in [-1, 1]$ is a random number and h is the local mesh size along the given dimension. The representative grids of classes A, B, and C are shown in Figures 1, 2, and 3, respectively.

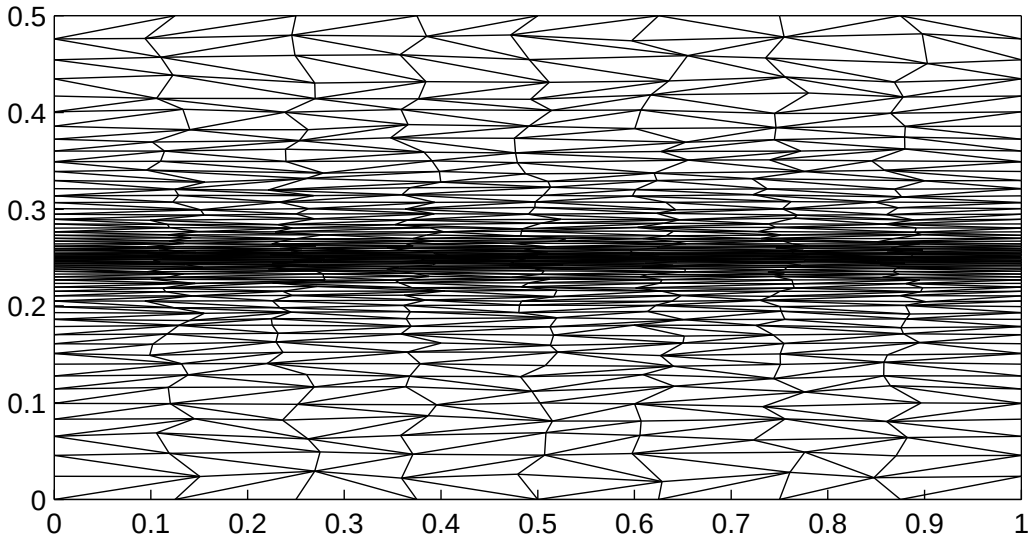

Figure 2. Class B: stretched grid of type (III_p) with 9×65 nodes.

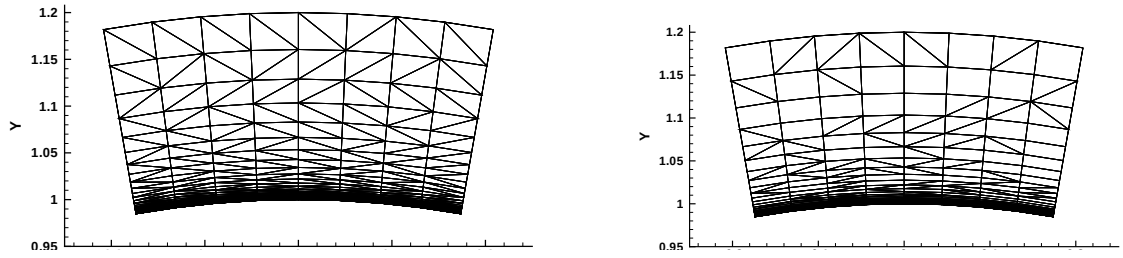

(a) **Grid of type (III).** (b) **Grid of type (IV).**

Figure 3. Class C: representative 9×33 irregular stretched high-Γ grids.

III. Finite-Volume Discretization Schemes

The FVD schemes are derived from the integral form of a conservation law,

$$\oint_{\partial\Omega} (\mathbf{F} \cdot \hat{\mathbf{n}})\, ds = \int_{\Omega} f d\Omega, \tag{3}$$

where Ω is a control volume with boundary $\partial\Omega$, $\hat{\mathbf{n}}$ is the outward unit normal vector, and ds is the area differential. The general FVD approach requires partitioning the domain into a set of non-overlapping control volumes and numerically implementing Eq. 3 over each control volume.

Node-centered discretization schemes are considered, in which solutions are defined at the primal mesh nodes. The control volumes are constructed around the mesh nodes by the median-dual partition. Node-centered discretization schemes have the same DOF on grids of all types.

For inviscid Eq. 1, the numerical flux,

$$\left(\mathbf{F}^{\mathbf{h}} \cdot \hat{\mathbf{n}}\right) \equiv U^h \left(\mathbf{a} \cdot \hat{\mathbf{n}}\right), \tag{4}$$

at a control-volume boundary is computed according to the flux-difference-splitting scheme,[26]

$$U^h \left(\mathbf{a} \cdot \hat{\mathbf{n}}\right) = \frac{1}{2} \left(U_L + U_R\right) \left(\mathbf{a} \cdot \hat{\mathbf{n}}\right) - \frac{1}{2} \left|\left(\mathbf{a} \cdot \hat{\mathbf{n}}\right)\right| \left(U_R - U_L\right), \tag{5}$$

where the first and second terms represent the flux average and the dissipation, respectively; U_L and U_R are the "left" and "right" solutions reconstructed at the edge midpoint by using solutions and gradients defined at the nodes connected by the edge. The edge-based flux integration scheme approximates the integrated flux through the two faces linked at the edge midpoint by $U^h \left(\mathbf{a} \cdot \mathbf{n}\right)$, where $\mathbf{n}$ is the combined directed-area vector of the adjacent faces.

The integration scheme is computationally efficient. For exact fluxes, the integration scheme provides third-order accuracy on regular simplicial grids of type (II), second-order accuracy on regular quadrilateral and general simplicial grids of types $(I), (III), (II_p)$, and (III_p), and first-order accuracy on mixed-element and perturbed quadrilateral grids of types $(IV), (IV_p)$, and (I_p).[18,19,27]

It was shown[23,24] that third order discretization accuracy is achieved on simplicial grids with WLSQ gradients employing a quadratic fit. Third-order accuracy on simplicial grids has been confirmed with quadratic-fit ULSQ gradients used herein. Note that five neighbors are typically sufficient for a quadratic fit. On triangular grids considered in this study, the average number of edge-connected neighbors is six; and the minimum number of edge-connected neighbors for an interior node on any grid is four. In cases when the least-squares stencil of the nearest edge-connected neighbors is not sufficient for a quadratic fit, the stencil is expanded to include neighbors of neighbors.

For viscous Eq. 2, the numerical flux is defined as

$$\left(\mathbf{F}^{\mathbf{h}} \cdot \hat{\mathbf{n}}\right) \equiv \left(\nabla^{\mathbf{r}} U \cdot \hat{\mathbf{n}}\right), \tag{6}$$

where $\nabla^{\mathbf{r}} U$ is the gradient reconstructed at the face of the control volume. Two gradient reconstruction schemes are considered. First, the averaged least-squares (Avg-LSQ) scheme averages the ULSQ gradients at the nodes to compute the face gradient.[28,29] Second, the GG scheme[15,22] computes gradients at the primal elements and uses them in face-gradient computations at control-volume boundaries. The GG scheme is widely used in node-centered codes and equivalent to a Galerkin finite-element (linear-element) discretization for triangular/tetrahedral grids. Both schemes use the edge gradient to augment the face gradient and increase the h-ellipticity[30] of the diffusion operator[15,21] and thus, avoid checkerboard instabilities. The gradient augmentation is introduced in the face-tangent form.[29] Note that when the edge is normal to the face, the edge gradient is the only contributor to the flux. For the GG scheme, the implementation of gradient augmentation on three-dimensional non-simplicial grids requires looping over elements and thus, alters the edge-based character of the scheme. The augmentation does not affect the face gradient within a simplex element and thus, the GG scheme is edge based on simplicial grids. Both Avg-LSQ and GG schemes possess second-order accuracy for viscous fluxes on general mixed-element grids.[18,19,28,29]

IV. Accuracy Measures

The accuracy is analyzed for known exact or manufactured solutions. The forcing function and boundary values are found by substituting this solution into the governing equations, including boundary conditions. The discrete forcing function is defined at the nodes that are not necessarily located at centroids of control volumes. Boundary conditions are over-specified, i.e., discrete solutions at boundary control volumes and, possibly, at their neighbors are specified from the manufactured solution. Unless described otherwise, the figures in this paper show accuracy measures versus an effective meshsize which is computed as the L_1 norm of the $\sqrt{V}$ function, where V is a measure of the control volume,

$$V = \int_{\Omega} d\Omega. \tag{7}$$

Relations between different methods of computing the effective meshsize are discussed in Ref. 19.

IV.A. Discretization error

The main accuracy measure is the *discretization error*, E_d, which is defined as the difference between the exact discrete solution, U^h, of the discretized Eq. 3 and the exact continuous solution, U, to the corresponding differential equations,

$$E_d = U - U^h, \tag{8}$$

where U is sampled at mesh nodes.

IV.B. Accuracy of gradient reconstruction

The accuracy of the gradient approximation is also important. The gradient reconstruction accuracy is evaluated by comparing the reconstructed gradient, $\nabla^{\mathbf{r}} U$, with the exact gradient, ∇U. The accuracy of a ULSQ gradient is evaluated by comparing the reconstructed and exact gradients at nodes. The accuracy of a GG gradient is evaluated at element centers computed as the average of the corresponding element vertexes. The error in the gradient reconstruction is measured as

$$E_{\mathrm{g}} = |\nabla^{\mathbf{r}} U - \nabla U|. \tag{9}$$

V. Class A: Isotropic Grids in Rectangular Geometry

V.A. Grid and solution specifications

Sequences of consistently refined[19] grids with $5^2, 9^2, 17^2, 33^2, 65^2, 129^2$, and 257^2 nodes are generated on the unit square $[0,1] \times [0,1]$. Irregularities are introduced at each grid independently, so the grid metrics remain discontinuous on all irregular grids. With the random perturbation range limited by a quarter of the local mesh size, the angles of triangular elements can approach 180° and the ratio of the neighboring cell volumes can be arbitrarily high.

The exact solution is $U = \sin(\pi x - 2\pi y)$, so for the inviscid Eq. 1 with $\mathbf{a} = (2,1)$, the force, f, is zero, and for the viscous Eq. 2, $f = -5\pi^2 \sin(\pi x - 2\pi y)$. The boundary conditions are over-specified from the manufactured solution for all nodes linked to the boundary.

V.B. Gradient reconstruction errors

Figure 4 shows the variation of the L_1 norm of the gradient error. As expected, the ULSQ gradient reconstruction with a quadratic fit is second-order accurate on all grids. The GG gradient reconstruction is second order only on perfect grids of type (I); on all other grids, the GG gradients are first-order accurate. All equivalent-order methods provide

very similar errors. Thus, no mesh regularity effects are observed for the L_1 norm of the gradient error on isotropic grids.

Although not shown, the observed L_∞ norms of the gradient errors converge with the same orders as the corresponding L_1 norms, but the L_∞ norms of GG gradient error on grids of types (III_p) and (IV_p) are an order of magnitude greater than the L_∞ norms of other first-order errors. The latter effect is caused by gradient accuracy deterioration on triangular elements with obtuse angles approaching $180°$. Theoretically, with an infinitesimal probability, the GG gradient error may become infinitely large at an element with a vanishing volume. As opposed to the anisotropic grids considered below, elements with extremely obtuse angles occur infrequently and in isolation on isotropic grids. Thus, discretization errors are not affected.

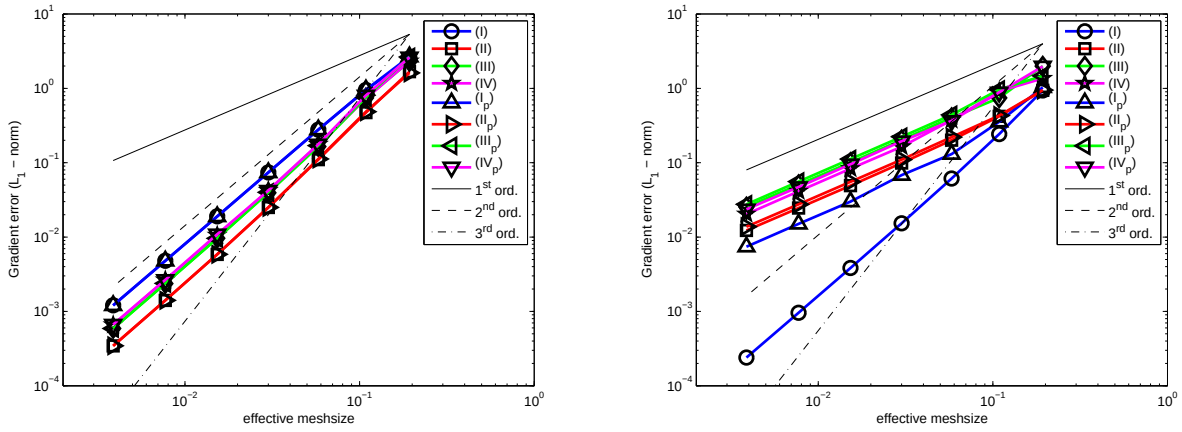

(a) **ULSQ-quadratic fit at node** (b) **GG at element**

Figure 4. Accuracy of gradient reconstruction on isotropic grids. Manufactured solution is $U = \sin(\pi x - 2\pi y)$.

V.C. Discretization errors

Convergence rates of the L_1 norm of discretization errors for inviscid and viscous fluxes are shown in Figures 5 and 6, respectively. This is an example where inviscid accuracy on simplicial meshes is superior to that on meshes with quadrilateral elements. This is not a surprise because the inviscid scheme used in this study is designed to be third order only on simplicial grids.[23,24] The edge-based integration scheme used in this scheme is known to deteriorate to first order on grids of types (I_p), (IV), and (IV_p).[18,19,27] On triangular grids, the discretization accuracy of inviscid solutions is not sensitive to mesh regularity. If anything, discretization errors are somewhat smaller on topologically structured grids of types (II) and (II_p). Discretization errors for viscous fluxes show no sensitivity to mesh regularity. The errors for both Avg-LSQ and GG schemes are practically identical to the plotting accuracy for all grids.

VI. Class B: Anisotropic Grids in Rectangular Geometry

VI.A. Grid and solution specifications

This section considers FVD schemes on stretched grids generated on rectangular domains. Figure 2 shows an example grid with the maximal aspect ratio $\mathcal{A} = 1,000$. A sequence of consistently refined stretched grids is generated on the rectangle $(x, y) \in [0, 1] \times [0, 0.5]$ in the following 3 steps.

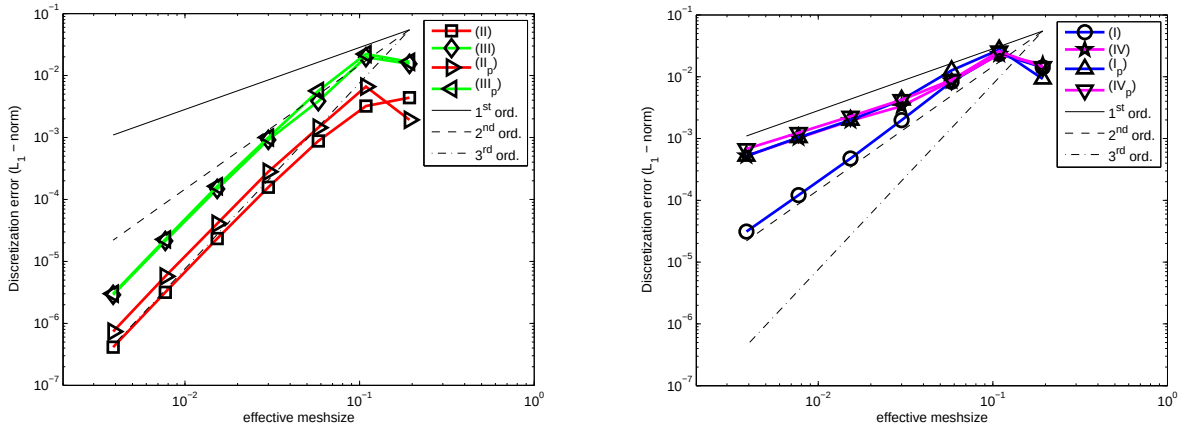

(a) **Triangular meshes** (b) **Mixed and quadrilateral meshes**

Figure 5. Inviscid discretization errors on isotropic grids. Manufactured solution is $U = \sin(\pi x - 2\pi y)$.

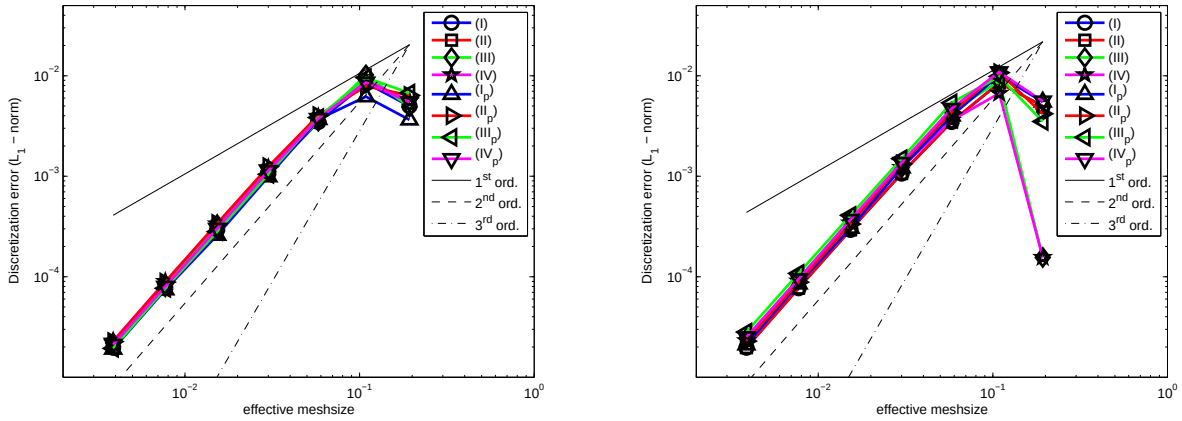

(a) **Avg-LSQ** (b) **GG**

Figure 6. Viscous discretization errors on isotropic grids. Manufactured solution is $U = \sin(\pi x - 2\pi y)$.

1. A background regular rectangular grid with $N = (N_x + 1) \times (N_y + 1)$ nodes and the horizontal mesh spacing $h_x = 1/N_x$ is stretched toward the horizontal line $y = 0.25$. The y-coordinates of the horizontal grid lines in the top half of the domain are defined as

$$y_{\frac{N_y}{2}+1} = 0.25; \qquad y_j = y_{j-1} + \hat{h_y}\beta^{j-\left(\frac{N_y}{2}+1\right)}, \qquad j = \frac{N_y}{2} + 2, \ldots, N_y, N_y + 1. \tag{10}$$

Here $\hat{h_y} = h_x/A$ is the minimal mesh spacing between the vertical lines, $\mathcal{A} = 1,000$ is a fixed maximal aspect ratio, and β is a stretching factor which is found from the condition $y_{N_y+1} = 0.5$. The stretching in the bottom half of the domain is defined analogously.

2. Irregularities are introduced by random shifts of interior nodes in the vertical and horizontal directions. The vertical shift is defined as $\Delta y_j = \frac{3}{16}\rho \min(h_y^{j-1}, h_y^j)$, where ρ is a random number between -1 and 1, and h_y^{j-1} and h_y^j are vertical mesh spacings on the background stretched mesh around the grid node. The horizontal shift is introduced analogously, $\Delta x_i = \frac{3}{16}\rho h_x$. With these random node perturbations, all perturbed quadrilateral cells are convex.

3. Each perturbed quadrilateral is randomly triangulated with one of the two diagonal choices; each choice occurs with a probability of one half.

Sequences of consistently refined stretched grids with maximum aspect ratio $\mathcal{A} = 1,000$ including $9 \times 65, 17 \times 129, 33 \times 257$, 65×513, and 129×1025 nodes have been considered. The corresponding stretching ratios are $\beta \approx 1.207, 1.098, 1.048, 1.025$, and 1.012. The aspect ratio near the external horizontal boundaries is about 2.7.

In the tests on grids of Class B performed with either the manufactured solution $\sin(\pi x - 2\pi y)$ or extended over-specification used in tests on grid of Class A, the asymptotic behavior of the discretizations errors for viscous fluxes was not observed on coarse grids. The exhibited discretization errors were uncharacteristically low on coarse grids, but did not converge with the asymptotic order. The discretization errors for this specific manufactured solution on the chosen domain are small in the interior and peak toward the boundary. Thus, over-specification that involves all neighbors of boundary nodes affects solutions on a too large portion of stretched grids. As a result, the manufactured solution has been changed to $U = \cos(\pi x - 2\pi y)$; the discretization errors for this solution peak in the middle of the computational domain. Also only solutions at boundary nodes are over-specified, and not at their neighbors as was done for Class A grids. With these changes, the asymptotic behavior of the discretizations errors for the viscous fluxes is established on relatively coarse grids. Note that the forcing term for inviscid equations is still $f = 0$ for $\mathbf{a} = (2, 1)$.

VI.B. Gradient reconstruction errors

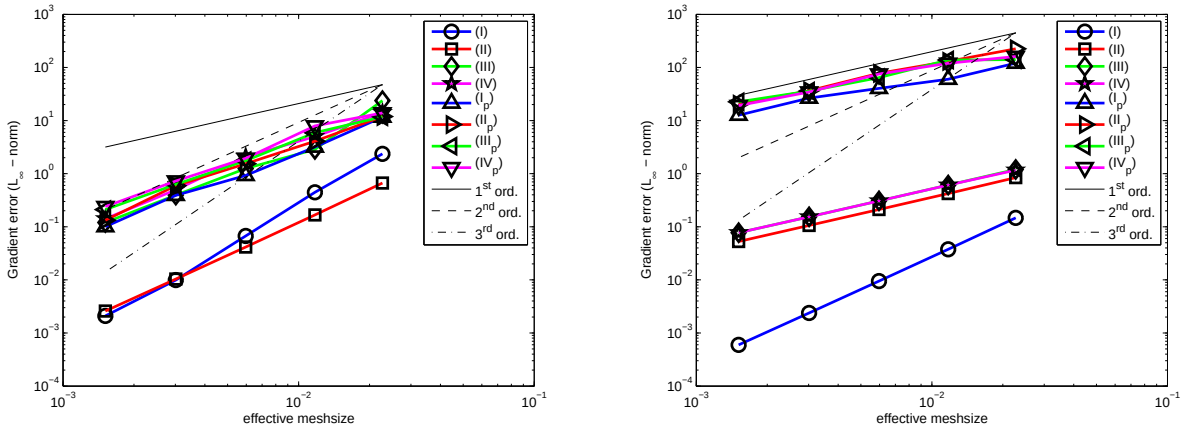

(a) **ULSQ-quadratic fit at node** (b) **GG at element**

Figure 7. Accuracy of gradient reconstruction on stretched grids with maximum aspect ratio $\mathcal{A} = 1,000$. Manufactured solution is $U = \cos(\pi x - 2\pi y)$.

A recent study[20] assessed the accuracy of gradient approximations on various grids with high aspect ratio $\mathcal{A} = \frac{h_x}{h_y} \gg 1$. The study indicates that for rectangular geometries and functions predominantly varying in the direction of

small mesh spacing (y-direction here), gradient reconstruction is accurate and provides small relative error while converging with at least first order in consistent refinement on grids of all types. For manufactured solutions significantly varying in the direction of larger mesh spacing (x-direction), the gradient reconstruction may produce extremely large relative errors $O(\mathcal{A}h_x^p)$ affecting the accuracy of the y-directional gradient component. Here, p is the formal gradient reconstruction order; $p = 1$ for the GG method and for the ULSQ method with a linear fit; $p = 2$ for the ULSQ scheme with a quadratic fit.

A summary of the results concerned with gradient accuracy on anisotropic grids is presented in Table 1. The gradient is accurately reconstructed on all unperturbed grids by the GG scheme. All gradient reconstruction methods considered may generate large relative errors on perturbed grids of types $(I_p) - (IV_p)$.

Table 1. Relative error of gradient reconstruction on anisotropic grids for solutions with significant variation in the x-direction of larger mesh spacing.

Grid Types	(I)	(II)	(III)	(IV)	$(I_p) - (IV_p)$
ULSQ-linear fit at node	$O(h_x^2)$	$O(h_x^2)$	$O(\mathcal{A}h_x)$	$O(\mathcal{A}h_x)$	$O(\mathcal{A}h_x)$
ULSQ-quadratic fit at node	$O(h_x^2)$	$O(h_x^2)$	$O(\mathcal{A}h_x^2)$	$O(\mathcal{A}h_x^2)$	$O(\mathcal{A}h_x^2)$
GG at element center	$O(h_x^2)$	$O(h_x)$	$O(h_x)$	$O(h_x)$	$O(\mathcal{A}h_x)$

The convergence of the L_∞ norm of gradient errors is shown in Figure 7. The L_∞ norm is used to highlight the worst gradients observed in high-aspect ratio regions of the stretched grids of Class B. All quadratic-fit ULSQ gradients converge with second order, but the magnitude of the gradient errors is sensitive to grid regularity. As shown in Table 1, with any deviation from the regularity of grids of types (I) and (II), the ULSQ gradient error becomes proportional to aspect ratio. The GG gradients converge with first order on all grids beside the grids of type (I), where a second-order convergence is observed. In spite of a lower order convergence, the GG gradients show a clear advantage over the ULSQ gradients on coarse unperturbed grids of types (I)–(IV). The GG scheme on such grids provides gradient accuracy independent of aspect ratio. On perturbed grids of types (I_p)–(IV_p), the GG errors are also proportional to the aspect ratio, and quadratic-fit ULSQ gradients are preferable.

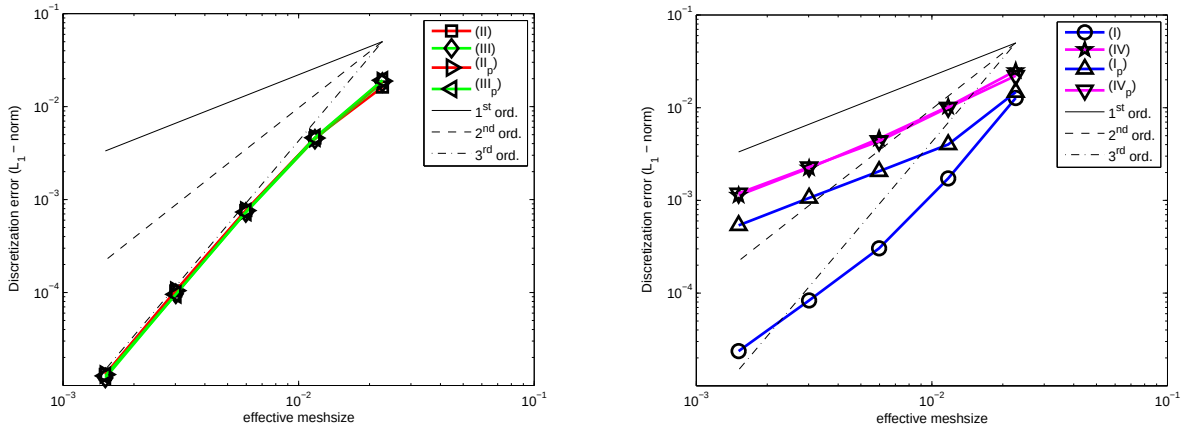

(a) **Triangular meshes** (b) **Mixed and quadrilateral meshes**

Figure 8. Inviscid discretization errors on anisotropic stretched grids with maximum aspect ratio $\mathcal{A} = 1,000$. Manufactured solution is $U = \cos(\pi x - 2\pi y)$.

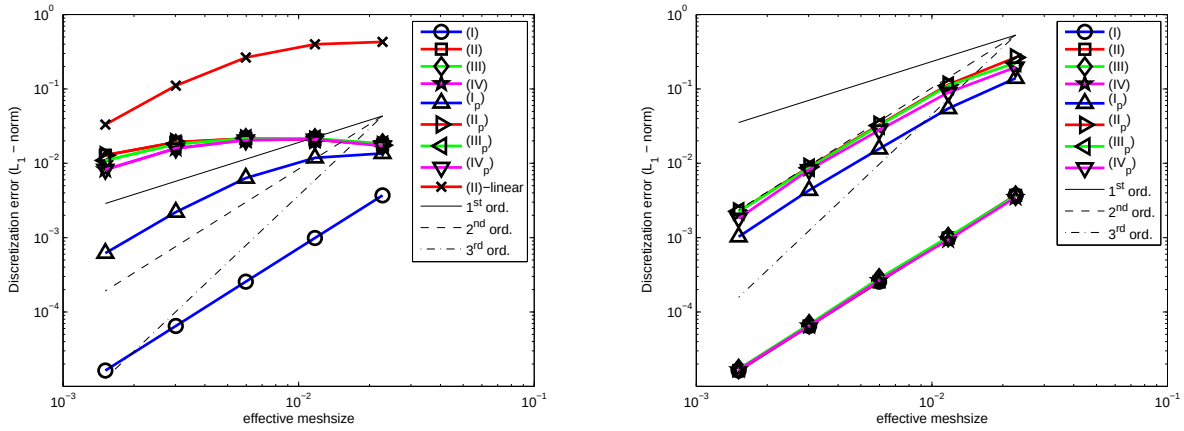

(a) **Avg-LSQ** (b) **GG**

Figure 9. Viscous discretization errors on anisotropic stretched grids with maximum aspect ratio $\mathcal{A} = 1,000$. Manufactured solution is $U = \cos(\pi x - 2\pi y)$.

VI.C. Discretization errors

The convergence of the L_1 norm of discretizations errors for inviscid fluxes is shown in Figure 8. The convergence characteristics are similar to those exhibited on isotropic grids of Class A. Third-order convergence insensitive to grid regularity is observed on all triangular grids. Convergence on grids of type (I) is second order, but any irregularity on mixed and quadrilateral meshes degrades the convergence to first order.

The convergence of the L_1 norm of discretization errors for viscous fluxes is shown in Figure 9. All discretization errors converge with second order. While second-order convergence of the Avg-LSQ scheme is not apparent in Figure 9(a) on triangular and mixed-element grids, a second-order slope has been attained on finer grids. For reference, convergence of the errors obtained with a linear fit on grids of type (II) is also shown. The Avg-LSQ errors are relatively small only on pure quadrilateral grids of types (I) and (I_p). The magnitude of errors obtained with a quadratic fit is much smaller than the magnitude of errors obtained with a linear fit. However, discretization errors of the GG scheme are significantly better than any of the Avg-LSQ errors. The GG errors are clearly divided into two groups. The errors on unperturbed grids of types $(I) - (IV)$ are small on all grids; the errors on perturbed grids are roughly two orders of magnitude higher for any given number of DOF. The ratio is about the same as the ratio between gradient errors shown in Figure 7(b).

VII. Class C: Grids with Curvature and High Aspect Ratio

VII.A. Grid and solution specifications

In this section, we discuss FVD schemes on grids with curvature and high aspect ratio. The grid nodes are generated from a cylindrical mapping, where (r, θ) denote polar coordinates with spacings of h_r and h_θ, respectively. The grid aspect ratio is defined as the ratio of mesh sizes in the circumferential and the radial directions, $\mathcal{A} = Rh_\theta/h_r$, where R is the radius of curvature.

The curvature-induced mesh deformation parameter Γ[15,16] is defined as:

$$\Gamma = \frac{R\,(1-\cos(h_\theta))}{h_r} \approx \frac{Rh_\theta^2}{2h_r} = \mathcal{A}\frac{h_\theta}{2}. \tag{11}$$

The following assumptions are made about the range of parameters: $R \approx 1$, $\mathcal{A} \gg 1$, and $\Gamma h_r \ll 1$, which implies that both h_r and h_θ are small. For a given value of $\mathcal{A}$, the parameter Γ may vary: $\Gamma \ll 1$ indicates meshes that are locally (almost) non-deformed. As a practical matter, grids with $\Gamma < 0.2$ can be considered as nominally non-curved. In a mesh refinement that keeps $\mathcal{A}$ fixed, $\Gamma = O(\mathcal{A}h_\theta)$ asymptotes to zero. This property implies that on fine enough grids with fixed curvature and aspect ratio, the error convergence is expected to be the same as on similar Class B grids generated on rectangular domains with no curvature.

Four basic types of grids are studied in the cylindrical geometry. Unlike Class B grids used in the rectangular geometry, random node perturbation is not applied to high-Γ grids of Class C because even small perturbations in the circumferential direction may lead to non-physical control volumes. Representative stretched grids of types (III) and (IV) are shown in Figure 3.

The manufactured solution considered in this section is $U = \sin(5\pi r)$. The convection direction is changed to a variable tangential direction $\mathbf{a} = (y/r^2, -x/r^2)$, so the inviscid forcing term remains zero. Solutions at boundary nodes are over-specified.

VII.B. Gradient reconstruction errors

Table 2. Relative errors of gradient reconstruction for manufactured solutions varying only in the radial direction on high-Γ grids.

Grid Types	(I)	(II)	(III)	(IV)
ULSQ-linear fit	$O(1)$	$O(1)$	$O(1)$	$O(1)$
ULSQ-quadratic fit	$O(h_\theta)$	$O(h_\theta)$	$O(h_\theta)$	$O(h_\theta)$
GG	$O(h_\theta^2)$	$O(h_\theta)$	$O(h_\theta)$	$O(h_\theta)$

Our main interest is solutions varying predominantly in the radial direction on grids with $\Gamma \gg 1$ corresponding to meshes with large curvature-induced deformation. The errors of gradient reconstruction for a radial solution are summarized in Table 2. The ULSQ gradient approximation with a linear fit is zeroth-order accurate for such solutions, in agreement with computations and analysis reported earlier.[17,25] The use of the ULSQ method with a quadratic fit dramatically improves gradient accuracy on high-Γ grids leading to a first-order convergence of gradient errors on grids with high Γ.

The computational tests are performed with downscaling[19,20] on a sequence of narrow arc-shaped domains with the angular extent of $\frac{\pi}{9}L$ radians and the radial extent of $1 \le r \le 1 + \frac{\pi}{9}L\mathcal{A}^{-1}$. The scale L changes as $L = 2^{-n}, n = 0, \ldots, 8$. On each domain, a 17×17 grid is generated with nodes uniformly spaced in the polar coordinates. Figure 10 shows convergence of the L_∞ norms of gradient errors computed for the manufactured solution $U = \sin(5\pi r)$ on grids with aspect ratios $\mathcal{A} = 100$ and $\mathcal{A} = 1,000$. The errors are shown versus the grid deformation parameter, Γ, defined in Eq. 11. Figures 10(a) and 10(b) show convergence of ULSQ gradient errors computed with quadratic and linear fits on grids of types (I)–(IV). Figures 10(c) and 10(d) show convergence of GG gradient errors. As known from previous studies,[15–17] the errors of GG gradients are small and show the order property on all grids. The ULSQ gradients computed with a linear fit lose accuracy on high-Γ grids. The ULSQ gradients computed with a quadratic fit recover a first-order convergence on high-Γ grids and show the smallest error magnitudes on grids of types $(II), (III)$, and (IV). The GG gradients show the smallest errors on regular quadrilateral grids of type (I). Appendix B presents a detailed study of gradient reconstruction errors for ULSQ methods with linear and quadratic fits on a family of stencils corresponding to a wide range of Γ.

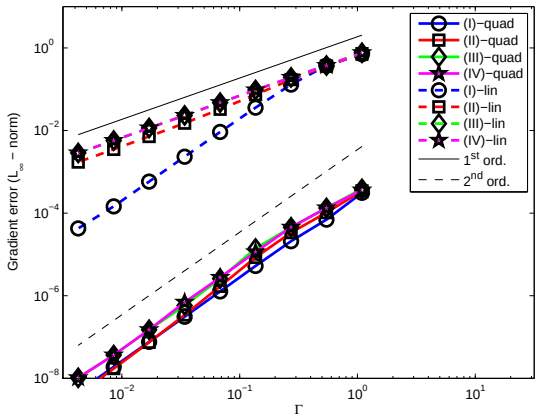

(a) **ULSQ at node,** $\mathcal{A} = 100$

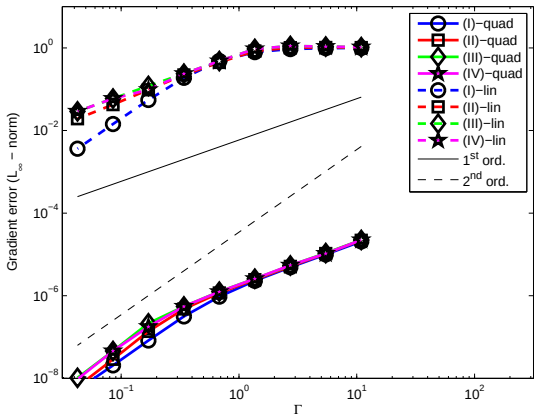

(b) **ULSQ at node,** $\mathcal{A} = 1,000$

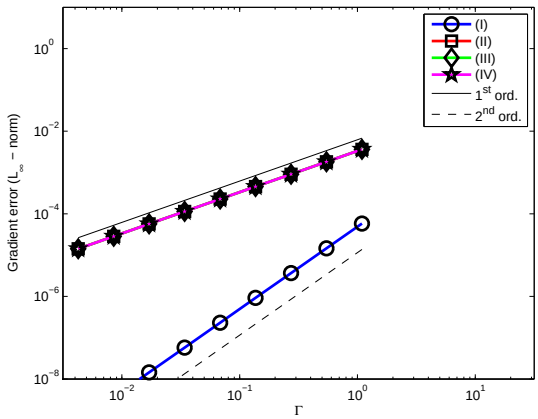

(c) **GG at element,** $\mathcal{A} = 100$

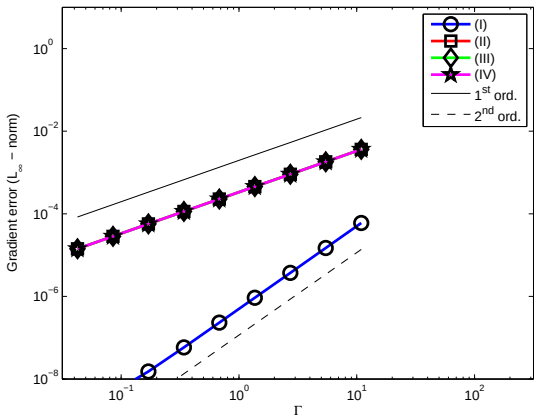

(d) **GG at element,** $\mathcal{A} = 1,000$

Figure 10. Accuracy of gradient reconstruction on high-Γ grids. Manufactured solution is $U = \sin(5\pi r)$.

VII.C. Discretization errors

Computational grids used in the grid-refinement study of discretization errors are radially stretched grids with a radial extent of $1 \leq r \leq 1.2$ and an angular extent of $20°$. Fixed maximal aspect ratios are used. The maximal aspect ratio is $\mathcal{A} \approx 1,000$ for viscous computations. The grids have four times more cells in the radial direction than in the circumferential direction. The maximum value of Γ changes approximately as $\Gamma \approx 22, 11, 5.5, \ldots$. The corresponding grid stretching ratios change as $\beta = 1.25, 1.11, 1.06, \ldots$.

The third-order inviscid scheme produces highly accurate solutions, so local errors become very small on relatively coarse highly stretched grids and convergence is obscured by round-off errors interfering with the solutions. A reduced maximal aspect ratio of $\mathcal{A} \approx 100$ has been chosen for inviscid computations.

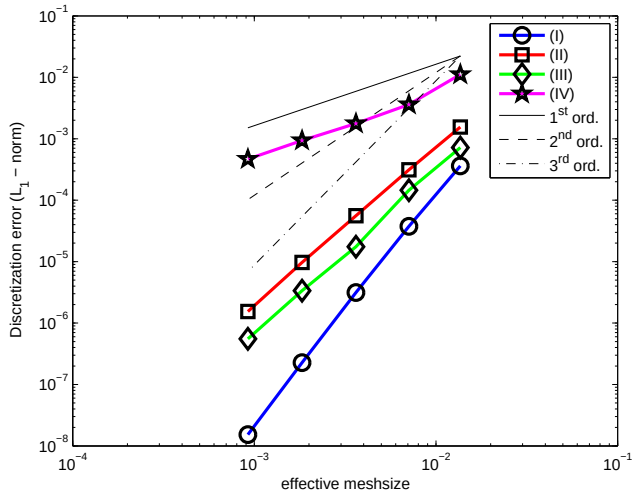

Figure 11. Inviscid discretization errors on high-Γ stretched grids with maximum aspect ratio $\mathcal{A} = 100$. Manufactured solution is $U = \sin(5\pi r)$.

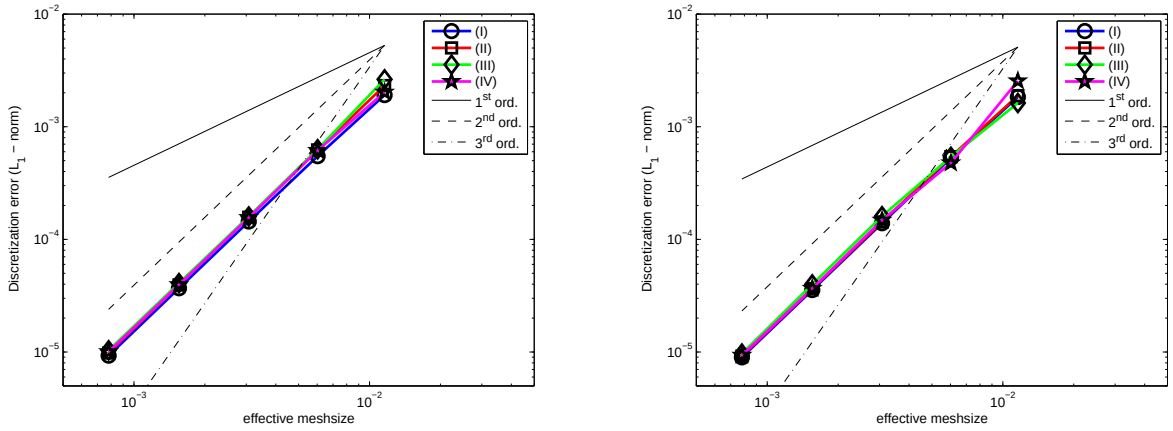

(a) **Avg-LSQ** (b) **GG**

Figure 12. Viscous discretization errors on high-Γ stretched grids with maximum aspect ratio $\mathcal{A} = 1,000$. Manufactured solution is $U = \sin(5\pi r)$.

Convergence of the L_1 norm of discretization errors is shown in Figures 11 and 12 for inviscid and viscous fluxes, respectively. The inviscid errors converge with (almost) fourth order on grids of type (I), with third order on grids of types (II) and (III), and with first order on grids of type (IV). The unusually high order of convergence on grids of type (I) is explained by the fact that, for a manufactured solution varying in the radial direction only, the inviscid scheme on grids of type (I) turns into a fourth-order pure one-dimensional scheme. Any solution variation in the circumferential direction results in the expected second-order convergence on grids of type (I). Note that, because of asymmetric gradient-reconstruction stencil on grids of types (II) and (III), the scheme does not become one-dimensional and thus, its third order of convergence on these grids is independent of solution variation. Second-order

convergence and no sensitivity to grid type are observed for both viscous schemes.

VIII. Conclusions

The effects of mesh regularity on the accuracy of unstructured node-centered finite-volume discretizations for viscous and inviscid fluxes have been considered for an edge-based approach that use unweighted least-squares gradient reconstruction with a quadratic fit. The inviscid scheme is nominally third-order accurate on general triangular meshes.[23,24] The viscous scheme is a nominally second-order accurate discretization that uses an average-least-squares method with a face-tangent augmentation.[28,29] The results have been contrasted with previously studied schemes involving other gradient reconstruction methods such as the Green-Gauss method and the unweighted least-squares method with a linear fit. Gradient errors, truncation errors, and discretization errors have been separately studied according to a previously introduced methodology.[15,16]

The methodology considers three classes of grids: Class A includes isotropic grids in a rectangular geometry, Class B includes anisotropic grids representative of adaptive-grid simulations, and Class C includes anisotropic advancing-layer grids representative of high-Reynolds number turbulent flow simulations over a curved body. Regular and irregular grids have been considered, including mixed-element grids and grids with random perturbations of nodes. Grid perturbations and stretching have been introduced independently of solution variation to bring out the worst possible behavior.

The gradient accuracy deteriorates on high-aspect-ratio perturbed grids. On grids of Class B, the gradient errors converge with the design orders – first order for the Green-Gauss method and the least-squares method with a linear fit and second order for the least-squares method with a quadratic fit. The least-squares gradient errors become proportional to the aspect ratio on all irregular grids. On grids with node perturbation, all gradient errors are proportional to the aspect ratio. On Class C grids characterized by a high deformation parameter Γ, the Green-Gauss gradient errors converge with at least first order and are small on all grids. The errors of least-squares gradients with a quadratic fit converge with first order. The magnitude of the quadratic-fit errors is superior to the $O(1)$ magnitude observed with a linear fit.

As observed previously[8–11,19] and confirmed here in Appendix A, lack of mesh regularity strongly affects truncation errors, which converge with lower-than-design order on all irregular meshes. Viscous truncation errors do not converge at all on perturbed grids.

Inviscid discretization errors are practically insensitive to mesh regularity on triangular grids, demonstrating a third-order convergence and small variation of the error magnitudes. Discretization accuracy is more sensitive to mesh regularity on grids with quadrilateral elements. On those grids, the results observed with the least-squares method with a quadratic fit show no advantage over previous results obtained with a linear fit,[16,19] both showing first-order convergence on mixed and perturbed quadrilateral grids.

In all cases, the viscous discretization errors asymptotically converge with second order. Similar to the gradient accuracy, the magnitude of discretization errors of viscous solutions is insensitive to grid regularity on grids of Class A, but may be sensitive on grids of classes B and C. On such grids, the Green-Gauss method is the most accurate, although the errors on the grids with node perturbation are still significantly larger than errors on grids with unperturbed nodes. Asymptotically, the difference is proportional to the aspect ratio. Accuracy of the average-least-squares methods deteriorates on irregular high-aspect-ratio grids, although the deterioration is less with a quadratic fit than with a linear fit.

The following recommendations are offered:

1. The unweighted least-squares method with a quadratic fit is highly recommended as a robust way to compute accurate gradients on all grids.

2. The edge-based scheme that uses the unweighted least-squares method with a quadratic fit is recommended for inviscid fluxes. On triangular grids, it produces third-order accurate solutions and is insensitive to mesh regularity.

3. The Green-Gauss scheme is recommended for viscous fluxes. On isotropic and advanced-layer grids of classes A and C, both Green-Gauss and averaged-least-squares methods produce uniformly second-order solutions and are insensitive to mesh regularity. On grids of Class B, there is a sensitivity to grid regularity; the Green-Gauss solutions are less sensitive than averaged-least-squares solutions.

Robust iterative convergence is also critically important for practical applications. The solver for the third-order scheme reported previously[23] failed to converge on high-Γ grids of Class C. This failure is attributed in part to use of a WLSQ gradient reconstruction that causes difficulties for iterative solvers in complex geometries.[25] Although, we do not consider iterative convergence in this paper, preliminary tests indicate that a combination of a ULSQ method with an approximate mapping technique[15,16] enables fast and robust convergence of defect-correction iterations for this third-order scheme on high-aspect-ratio grids in complex geometries. Also, the approximate-mapping approach to gradient reconstruction can recover a second-order convergence of gradient errors on high-Γ grids of Class C.

The overall conclusion is that relations between mesh characteristics and solution accuracy are complicated. The mesh regularity affects gradient, truncation, and discretization errors in dramatically different ways. The resolution is expected in the form of adjoint-based grid adaptation that directly and rigorously connects the local mesh properties with the desired solution outcome.

A. Truncation errors

Truncation error, E_t, characterizes the accuracy of approximating the differential equations. For finite differences, the truncation error is defined as the residual obtained after substituting the exact solution U into the discretized differential equations.[31] For FVD schemes, the traditional truncation error is usually defined from the time-dependent standpoint.[32,33] In the steady-state limit, it is defined (e.g., in Ref. 34) as the residual computed after substituting U into the normalized discrete Eq. 3,

$$E_t = \frac{1}{V}\left[-\int_{\Omega} f^h \, d\Omega + \oint_{\partial\Omega} \left(\mathbf{F^h} \cdot \hat{\mathbf{n}} \right) \, ds \right], \tag{12}$$

where V is the measure of the control volume, Eq. 7, f^h is an approximation of the forcing function f on Ω, and the integrals are computed according to quadrature formulas.

The truncation errors are extremely sensitive to mesh regularity. Convergence rates of the L_1 norm of truncation errors for inviscid and viscous fluxes on isotropic grids of Class A are shown in Figures 13 and 14, respectively. The inviscid scheme and the viscous Avg-LSQ scheme use the ULSQ method with a quadratic fit; the viscous GG scheme is shown for comparison. The grids and manufactured solution are defined in Section V.A.

The inviscid errors converge with third order only on regular triangular meshes of type (II). On irregular triangular grids of types $(III), (II_p)$, and (III_p) and on perfect quadrilateral grid of type (I), the inviscid truncation errors converge with second order. Irregularities on grids with quadrilateral elements (types (IV), (I_p), and (IV_p)) lead to zeroth-order convergence.

Similar sensitivity is observed for the truncation errors of viscous fluxes discretized by the Avg-LSQ scheme with second-order accurate ULSQ gradients (Figures 14(a) and 14(b)). The second-order convergence is observed only on perfectly regular grids of types (I) and (II). The convergence deteriorates to first order on irregular triangular grids and to zeroth order on mixed-element and perturbed quadrilateral grids. For viscous fluxes discretized with the GG scheme (Figures 14(c) and 14(d)), truncation errors do not converge on any but perfectly regular grids of types (I) and (II). Note that GG scheme produces identical discretizations on grids of types $(I), (II)$, and (III).[15] Thus, corresponding GG solutions and truncation errors on grids of types (I) and (II) are always identical. Different results on grids of type (III) are explained by the differences in the dual volumes.

The qualitative behavior (orders of convergence) of truncation errors on anisotropic grids of Class B is the same as on isotropic grids, shown in Figures 13 and 14. On grids with similar DOF, the magnitude of the errors increases

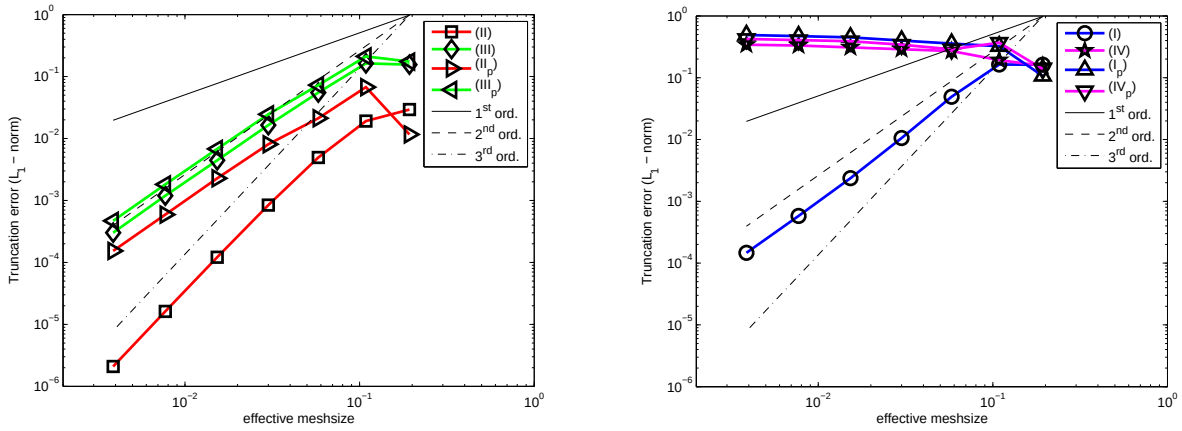

(a) **Triangular grids** (b) **Mixed and quadrilateral grids**

Figure 13. Inviscid truncation errors on isotropic grids. Manufactured solution is $U = \sin(\pi x - 2\pi y)$.

proportional to the aspect ratio.

B. Variation of gradient errors on grids of Class C

Table 3. Stencil for study of accuracy of gradient reconstruction on highly deformed grids.

Point	r	θ	x	y
0	R	0	0	0
N	$R+h_r$	0	0	h_r
S	$R-h_r$	0	0	$-h_r$
E	R	h_θ	$R\sin(h_\theta)$	$-R(1-\cos(h_\theta))$
W	R	$-h_\theta$	$-R\sin(h_\theta)$	$-R(1-\cos(h_\theta))$
NE	$R+h_r$	h_θ	$(R+h_r)\sin(h_\theta)$	$-(R+h_r)(1-\cos(h_\theta))$
SW	$R-h_r$	$-h_\theta$	$-(R-h_r)\sin(h_\theta)$	$-(R-h_r)(1-\cos(h_\theta))$

To illustrate the convergence property of gradient errors over a wide range of the deformation parameter Γ, a special computational test is designed. In the test, the gradient reconstruction is performed on a seven-point stencil corresponding to a Type (II) curved grid. The positions of stencil points (labeled in the compass notation) are shown in Table 3 in polar coordinates (r, θ) and in Cartesian coordinates (x, y) relative to the stencil center. In this test, radius $R = 1$ and radial mesh spacing $h_r = 2.5 \cdot 10^{-8}$ are kept fixed, the initial value of angular mesh spacing $h_\theta \approx 0.04$ is reduced by factor 2 in each of 13 refinement steps. With this "semi-refinement", Γ is reduced by factor 4 in each step, varying as $40,000 > \Gamma > 0.0005$ over the entire test. Figure 15 shows convergence of the Taylor expansion coefficients for the y-component of the gradient. The coefficients of terms that are not present in the figure are smaller than 10^{-10}. For the Taylor coefficients of the ULSQ y-gradient with a linear fit, a large magnitude and a flat convergence of the coefficient of U_{xx} observed in Figure 15(a) for $\Gamma \geq 1$ confirm an $O(1)$ accuracy of this gradient reconstruction method. In contrast, all Taylor coefficients of the ULSQ y-gradient with a quadratic fit shown

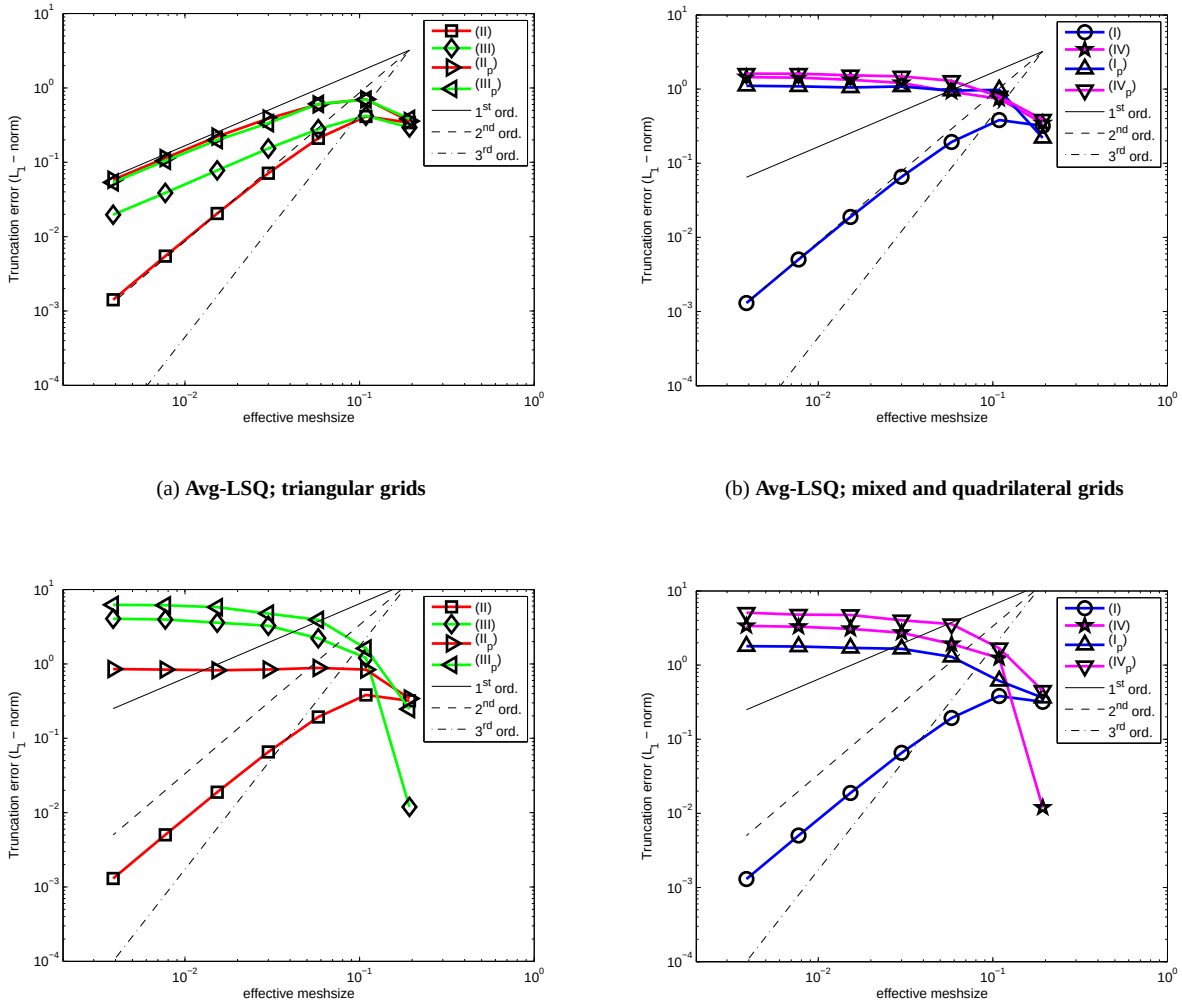

(a) **Avg-LSQ; triangular grids**

(b) **Avg-LSQ; mixed and quadrilateral grids**

(c) **GG; triangular grids**

(d) **GG; mixed and quadrilateral grids**

Figure 14. Viscous truncation errors on isotropic grids. Manufactured solution is $U = \sin(\pi x - 2\pi y)$.

in Figure 15(b) are small and converge with at least first order for high-Γ stencils.

The magnitudes of the relative errors for the GG scheme and for the ULSQ scheme with a quadratic fit are much smaller than the magnitude for the ULSQ scheme with a linear fit. Figure 16 shows the gradient errors measured at the center of the stencil for a radial solution $U = \sin(5\pi r)$. The gradient errors in Figure 16(a) confirm lack of accuracy for the ULSQ method with a linear fit on high-Γ grids. Low errors and flat convergence of the ULSQ method with a quadratic fit observed in Figure 16(b) are expected for accurate gradient reconstructions because the radial mesh size does not decrease in the test. This behavior indicates that for solutions varying predominantly in the radial direction, the gradient accuracy is determined by the radial mesh spacing and independent of Γ, which is a highly desirable property on high-Γ grids.

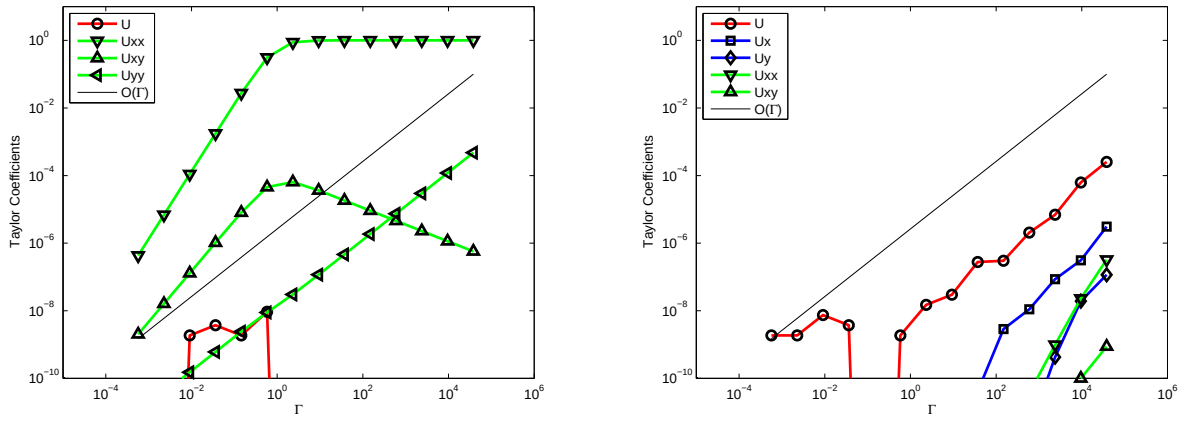

(a) **ULSQ linear fit** (b) **ULSQ quadratic fit**

Figure 15. Convergence of Taylor coefficients in semi-refinement test.

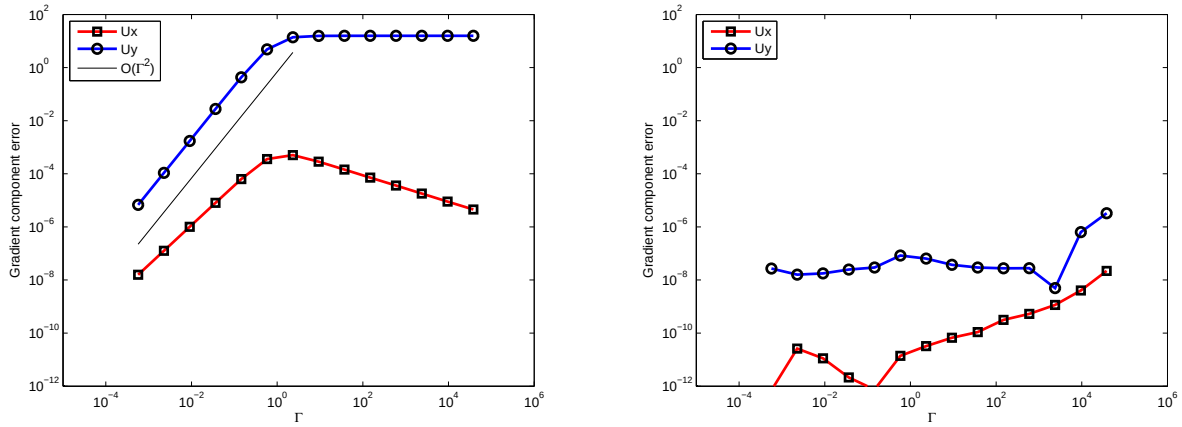

(a) **ULSQ linear fit** (b) **ULSQ quadratic fit**

Figure 16. Convergence of gradient errors in semi-refinement test.

References

[1]Fidkowski, K. J. and Darmofal, D. L., "Review of Output-Based Error Estimation and Grid Adaptation in Computational Fluid Dynamics," *AIAA Journal*, Vol. 49, No. 4, 2011, pp. 673–694.

[2]Park, M., Lee-Rausch, E. M., and Rumsey, C. L., "FUN3D and CFL3D Computations for the First High Lift Prediction Workshop," AIAA Paper 2011-936, January 2011.

[3]Berzins, M., "Mesh Quality: A function of Geometry, Error Estimates, or Both?" *Engineering with Computers*, Vol. 15, No. 3, 1999, pp. 236–247.

[4]Knupp, P. M., "Algebraic Mesh Quality Measures," *SIAM J. Sci. Comp.*, Vol. 23, No. 1, 2001, pp. 193–218.

[5]Knupp, P. M., "Remarks on Mesh Quality," Oral presentation, 45-th AIAA Aerospace Science Meeting and Exhibit, Reno, NV, January 2007.

[6]Mastin, C. W., "Error induced by coordinate system," *Numerical Grid Generation*, edited by J. Thompson, North-Holand, New York, 1982, pp. 31–40.

[7]Lee, J. and Tsuei, Y., "A Formula for Estimation of Truncation Errors of Convection Terms in a Curvilinear Coordinate System," *J. Comput. Phys.*, Vol. 98, 1992, pp. 90–100.

[8]Diskin, B. and Thomas, J. L., "Notes on Accuracy of Finite Volume Discretization Schemes on Irregular Grids," *Appl. Num. Math.*, Vol. 60, No. 3, 2009, pp. 224–226, doi: 10.1016/j.apnum.2009.12.001.

[9]Forsyth, P. A. and Sammon, P. H., "Quadratic convergence for cell-centered grids," *Appl. Num. Math.*, Vol. 4, 1988, pp. 377–394.

[10]Kreiss, H. O., Manteuffel, T. A., Wendroff, B., and White, A. B., "Supra-convergence schemes on irregular grids," *Mathematics of Computations*, Vol. 47(176), October 1986, pp. 537–554.

[11]Manteuffel, T. A. and White, A. B., "The numerical solution of the second-order boundary value problem on nonuniform meshes," *Mathematics of Computations*, Vol. 47, No. 176, 1986, pp. 511–536.

[12]Babushka, I. and Aziz, A. K., "On the angle condition in the finite element method," *SIAM J. Numer. Anal.*, Vol. 13, April 1976, pp. 214–226.

[13]Krizek, M., "On the maximum angle condition for linear tetrahedral elements," *SIAM J. Numer. Anal.*, Vol. 29, No. 2, April 1992, pp. 513–520.

[14]Berzins, M., "Solution-Based Mesh Quality Indicators for Triangular and Tetrahedral Meshes," *International Journal of Computational Geometry and Applications*, Vol. 10, No. 3, 2000, pp. 333–346.

[15]Diskin, B., Thomas, J. L., Nielsen, E. J., Nishikawa, H., and White, J. A., "Comparison of Node-Centered and Cell-Centered Unstructured Finite-Volume Discretizations: Viscous Fluxes," *AIAA Journal*, Vol. 48, No. 7, 2010, pp. 1326–1338.

[16]Diskin, B. and Thomas, J. L., "Comparison of Node-Centered and Cell-Centered Unstructured Finite-Volume Discretizations: Inviscid Fluxes," *AIAA Journal*, Vol. 49, No. 4, 2011, pp. 836–854.

[17]Mavriplis, D. J., "Revisiting the Least-Square Procedure for Gradient Reconstruction on Unstructured Meshes," AIAA Paper 2003-3986, June 2003.

[18]Diskin, B. and Thomas, J. L., "Accuracy Analysis for Mixed-Element Finite-Volume Discretization Schemes," NIA Report 2007-08, August 2007.

[19]Thomas, J. L., Diskin, B., and Rumsey, C. L., "Towards Verification of Unstructured-Grid Solvers," *AIAA Journal*, Vol. 46, No. 12, 2008, pp. 3070–3079.

[20]Diskin, B. and Thomas, J. L., "Accuracy of Gradient Reconstruction on Grids with High Aspect Ratio," NIA Report 2008-12, December 2008.

[21]Haselbacher, A. C., *A Grid-Transparent Numerical Method for Compressible Viscous Flow on Mixed Unstructured Meshes*, Ph.D. thesis, Loughborough University, 1999.

[22]Anderson, W. K. and Bonhaus, D. L., "An implicit upwind algorithm for computing turbulent flows on unstructured grids," *Computers and Fluids*, Vol. 23, No. 1, 1994, pp. 1–21.

[23]Katz, A. and Sankaran, V., "Mesh quality effects on the accuracy of Euler and Navier-Stokes solutions on unstructured meshes," *Journal of Computational Physics*, Vol. 230, No. 20, 2011, pp. 7670–7686.

[24]Katz, A. and Sankaran, V., "An Efficient Correction Method to Obtain a Formally Third-Order Accurate Flow Solver for Node-Centered Unstructured Grids," *Journal on Scientific Computing*, 2011, doi: 10.1007/s10915-011-9515-1.

[25]Smith, T. M., Barone, M. F., Bond, R. B., Lorber, A. A., and Baur, D. G., "Comparison of Reconstruction Techniques for Unstructured Mesh Vertex Centered Finite Volume Scheme," AIAA Paper 2007-3958, June 2007.

[26]Roe, P. L., "Approximate Riemann solvers, parameter vectors, and difference schemes," *J. Comp. Phys.*, Vol. 43, No. 2, 1981, pp. 357–372.

[27]Aftosmis, M., Gaitonde, D., and Tavares, T. S., "Behavior of linear reconstruction techniques on unstructured meshes," *AIAA Journal*, Vol. 33, No. 11, 1995, pp. 2038–2049.

[28]Nishikawa, H., Diskin, B., and Thomas, J. L., "Critical study of agglomerated multigrid methods for diffusion," *AIAA Journal*, Vol. 48, No. 4, 2010, pp. 839–847.

[29]Thomas, J. L., Diskin, B., and Nishikawa, H., "A Critical Study of Agglomerated Multigrid Methods for Diffusion on Highly-Stretched Grids," *Computers and Fluids*, Vol. 41, No. 1, 2011, pp. 82–93.

[30]Trottenberg, U., Oosterlee, C. W., and Schüler, A., *Multigrid*, Academic Press, London, 2000.

[31]Hirsch, C., *Numerical computation of internal and external flows. Vol.1, Fundamentals of numerical discretization*, A Wiley-Interscience publication, John Wiley & Sons, Inc., New York, NY, USA, 1988.

[32]Syrakos, A. and Goulas, A., "Estimate of the Truncation Error of Finite Volume Discretization of the Navier-Stokes Equations on Collocated Grids," *Int. J. Numer. Meth. Fluids*, Vol. 50, No. 1, 2006, pp. 103–130.

[33]Turkel, E., "Accuracy of Schemes with Nonuniform Meshes for Compressible Fluid Flows," *Applied Numerical Mathematics*, Vol. 2, No. 6, 1986, pp. 529–550.

[34]Giles, M. B., "Accuracy of node-based solutions on irregular meshes," *11th International Conference on Numerical Methods in Fluid Dynamics*, edited by D. L. Dwoyer, M. Y. Hussaini, and R. Voigt, Lecture Notes in Physics, v. 323, Springer-Verlag, 1989, pp. 369–373.